High Dynamic Polarization of Protons*

T. J. SCHMUGGE† AND C. D. JEFFRIES
Department of Physics, University of California, Berkeley, California
(Received 21 January 1965)

This paper is a detailed study of the dynamic polarization of the protons in the waters of hydration in the crystal $(Nd, La)_2Mg_3(NO_3)_{12}\cdot 24H_2O$, which occurs when one saturates a microwave "forbidden" transition that simultaneously flips a proton and a Nd^{3+} ion. The proton relaxation, as well as the dynamics of the polarization process, is discussed in terms of a phenomenological shell-of-influence model. A polarization apparatus is described for use at frequencies up to 75 kMc/sec and temperatures $1.3<T<4.2$°K. Proton relaxation rates T_{1p}^{-1} are measured over a wide range of fields H and temperatures, and are found to be in agreement with the predicted rate $T_{1p}^{-1}\approx T_{1e}^{-1}(g_{Nd}\beta/H)^2\langle r^{-6}\rangle_{av}$, where T_{1e}^{-1} is the relaxation rate for the Nd^{3+} ion, r is the separation between proton and ion, and the average is taken over the shell of influence. At the Nd concentration studied (~1%), the local fields apparently prevent the free diffusion of spin temperature. Dynamic proton polarization measurements are made over a wide range of frequencies and temperatures: at 75 kMc/sec and 1.5°K a polarization of at least 70% is observed. At these high polarizations, the proton magnetic-resonance line shape changes and a structure appears, due to the freezing-in of the local dipolar fields. At still higher polarizations a local-field computation predicts a series of sharp proton lines, suggesting the possibility of high-resolution nuclear magnetic resonance in solids. The crystal studied is a favorable one for construction of polarized proton targets.

I. INTRODUCTION

BY extending earlier work[1,2] to higher microwave frequencies and magnetic fields we have shown that polarizations of at least 70% may be obtained for the protons in the waters of hydration of the lanthanum magnesium nitrate crystal $La_2Mg_3(NO_3)_{12}\cdot 24H_2O$ ("LaMN") containing a small fraction of neodymium.[3] From the viewpoint of magnetic resonance this substance appeared to be a rather favorable one for the production of highly polarized samples and has subsequently been used successfully in the construction of sizable polarized proton targets.[4,5] In this paper we will not be concerned with the nuclear aspects of targets, but rather with the detailed spin-phonon dynamics of the crystals, i.e., relaxation processes, the dynamic polarization process, the magnitude of the polarization, and its build up and decay. The treatment is intended to be comprehensible to the nonspecialist.

In Sec. II we review briefly the method[6,7] of dynamic orientation used in these experiments, utilizing an elementary phenomenological approach to predict the dynamical behavior. Section III describes the apparatus we have used at helium temperatures with frequencies up to 75 kMc/sec and fields up to 22 kOe. For Nd^{3+} in LaMN we present measurements and interpretation of the proton spin-lattice relaxation in Sec. IV, and dynamic polarization in Sec. V. Some of these results have been briefly reported earlier.[2,3,8,9]

II. SIMPLE MODELS OF DYNAMIC POLARIZATION

This discussion is generally applicable to a system of electron spins $\mathbf{S}$ and nuclear spins $\mathbf{I}$ in weak dipolar coupling in a solid and in a large external magnetic field H. However, to fix ideas, we think of the specific system for which measurements are later presented, a single crystal of LaMN in which a small fraction, ~1%, of the La^{3+} ions have been replaced by paramagnetic Nd^{3+} ions added to the crystal growing solution. At low temperatures we may picture the Nd ion as an isolated "electron spin" with angular momentum $\hbar\mathbf{S}$ and magnetic dipole moment $-g\beta\mathbf{S}$; $S=\frac{1}{2}$=effective spin, β=Bohr magneton, and the anisotropic g factor has the principal values $g_{\parallel}=0.36$ and $g_{\perp}=2.70$ for the crystal axis $z'\parallel H$ and $z'\perp H$, respectively.[10] The Nd ions form our electron spin system. We take our nuclear spin system to be the relatively abundant protons in the 24 waters of hydration, characterized by nuclear spin $I=\frac{1}{2}$, and magnetic-dipole moment $g_n\beta\mathbf{I}$, with a nuclear g factor $g_n=+0.00304$. We imagine the crystal to be enclosed in a copper microwave cavity, immersed in liquid He^4 at a temperature $T\sim 1$°K, and in an external field $H\sim 10^4$ Oe. Figure 1 shows the over-all experimental arrangement to keep in mind, including an rf coil wound around the crystal for observing the nuclear

* Supported in part by the U. S. Atomic Energy Commission and the U. S. Office of Naval Research.
† Now at Trinity College, Hartford, Connecticut.
[1] O. S. Leifson and C. D. Jeffries, Phys. Rev. **122**, 1781 (1961).
[2] T. J. Schmugge and C. D. Jeffries, Phys. Rev. Letters **9**, 268 (1962).
[3] C. D. Jeffries, *Dynamic Nuclear Orientation* (John Wiley & Sons, Inc., New York, 1963).
[4] O. Chamberlain, C. D. Jeffries, C. H. Schultz, G. Shapiro, and L. Van Rossum, Phys. Letters **7**, 293 (1963); G. Shapiro, *Progress in Nuclear Techniques and Instrumentation* (North Holland Publishing Company, Amsterdam, 1964), Vol. 1; C. H. Schultz, Lawrence Radiation Laboratory Report No. UCRL 11149, 1964, (unpublished); O. Chamberlain, C. Schultz, and G. Shapiro, in Proceedings of the 1964 International Conference on High Energy Physics, Dubna, USSR (unpublished).
[5] M. Borghini, M. Odehnal, P. Roubeau, C. Ryter, G. Coignet, L. Dick, and L. di Lella, in Proceedings of the 1964 International Conference on High Energy Physics, Dubna, USSR (unpublished).
[6] A. Abragam and W. G. Proctor, Compt. Rend. **246**, 2253 (1958).
[7] C. D. Jeffries, Phys. Rev. **106**, 164 (1957); **117**, 1056 (1960).
[8] C. D. Jeffries, Ann. Rev. Nucl. Sci. **14**, 101 (1964).
[9] C. D. Jeffries, Proc. Roy. Soc. (London) **A283**, 471 (1965).
[10] A. H. Cooke and H. J. Duffus, Proc. Roy. Soc. (London) **A229**, 407 (1955); The g factors we use are later measurements by P. L. Scott (Ref. 14).

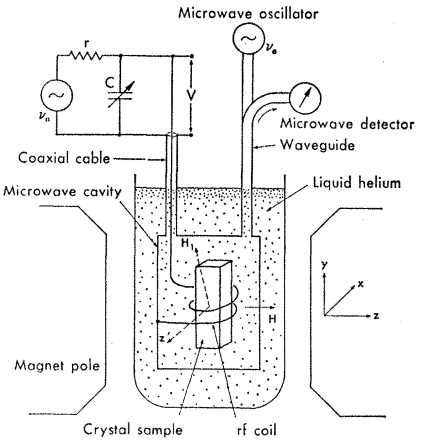

FIG. 1. Experimental arrangement for dynamic proton polarization.

magnetic resonance (nmr) and hence the polarization. We introduce crystal coordinates (x',y',z'), and laboratory coordinates (x,y,z), with $\mathbf{H}\|\hat{z}$; the orientation of $\mathbf{H}$ with respect to (x',y',z') is given by the usual spherical coordinates $\theta=\angle z'$, H and $\varphi=\angle x'$, $H_\perp$ (cf. Fig. 10).

The protons are dynamically polarized when one induces "forbidden" microwave transitions at frequency ν_e which simultaneously flip proton spins and Nd^{3+} spins through their weak dipolar coupling. Our objective is to calculate the sample-average proton polarization $p=\langle I_z\rangle_{av}/I$ and its transient behavior under the simultaneous action of the applied microwave field and the relaxation processes arising from the crystal lattice thermal vibrations. Our treatment should be valid even for $h\nu_e/kT\gg1$, necessary for very high polarizations. This is actually a very complex problem: we have a many-spin system in which the protons greatly outnumber the Nd ions, which are randomly distributed at the crystal lattice sites. Besides this complicated geometrical arrangement there is the further fact that at the large microwave fields required to strongly induce the forbidden transitions, simple perturbation theory and rate equations are not entirely valid. A proper approach is through the density matrix formulation.[11–13] However the exact results do not differ greatly from simpler theory if the forbidden lines are well resolved, as they are in the high fields and frequencies we use. This is the case we consider, using a simple phenomenological approach, hoping thereby to retain physical significance in the analysis.

A. Single Typical Pair Model

We further simplify the geometry of the problem for the moment by considering just one Nd ion **S** and one neighboring proton **I** separated by **r**. Introducing the **g** tensor for the Nd ion we write the static spin Hamiltonian for this typical pair

$$\mathcal{H}=\beta\mathbf{H}\cdot\mathbf{g}\cdot\mathbf{S}-\beta g_n\mathbf{H}\cdot\mathbf{I}-\frac{g_n\beta^2}{r^3}\times\left[\mathbf{I}\cdot\mathbf{g}\cdot\mathbf{S}-3\frac{(\mathbf{r}\cdot\mathbf{I})(\mathbf{r}\cdot\mathbf{g}\cdot\mathbf{S})}{r^2}\right]. \quad (1)$$

The terms represent the Nd Zeeman, proton Zeeman, and dipole-dipole $\mathcal{H}_{dd}$ interactions, respectively. We further specialize to the orientation $z'\|x$, i.e., $\theta=90°$. The g factor is maximized for this orientation, the linewidth is a minimum, and, for a fixed magnetic field, allows the use of the maximum microwave frequency, yielding the maximum polarization in the ideal case. Since the last term is negligible the states are well characterized by the zero-order wave functions $|M,m\rangle^0$, where $M=\langle S_z\rangle=\pm\frac{1}{2}$, and $m=\langle I_z\rangle=\pm\frac{1}{2}$. The four energy levels $E(M,m)=g_\perp\beta HM-g_n\beta Hm$ are shown in Fig. 2.

Transitions between these levels may be induced by connecting a microwave oscillator via a waveguide to the cavity, Fig. 1, which produces a field of components $(H_{1x},H_{1y},H_{1z})\cos2\pi\nu_e t$. This field will induce $\Delta M=1$, $\Delta m=0$ paramagnetic resonance (epr) transitions at the rate[7]:

$$W_1=(T_{2e}\beta^2/8\hbar^2)(H_{1x}^2g_{11}^2+H_{1y}^2g_\perp^2)\ \text{sec}^{-1}, \quad (2a)$$

where T_{2e} is the inverse paramagnetic resonance linewidth $(2\pi\Delta\nu_e)^{-1}$. Since $g_{11}^2\ll g_\perp^2$ for Nd^{3+} we note that the H_{1y} component is most important. Defining $H_{1y}=2H_{1e}$, $g_\perp\beta/\hbar=\gamma_e$, Eq. (2a) takes the familiar form

$$W_1=\tfrac{1}{2}T_{2e}(\gamma_eH_{1e})^2\ \text{sec}^{-1}. \quad (2b)$$

The term $S_z(I_x\pm iI_y)$ in $\mathcal{H}_{dd}$ admixes the states slightly

$$|M,m\rangle\approx|M,m\rangle^0+d_\pm|M,m\pm1\rangle^0,$$

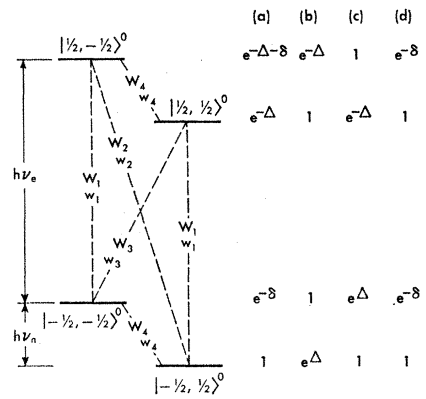

FIG. 2. Energy levels; states $|M,m\rangle^0$; oscillator-induced transitions W_1, $\cdots$; relaxation transitions w_1, $\cdots$; and populations for a proton and a Nd^{3+} ion in a magnetic field.

[11] A. G. Redfield, Phys. Rev. **98**, 1787 (1955).
[12] B. N. Provotorov, Zh. Eksperim. i Teor. Fiz. **41**, 1582 (1961) [English transl.: Soviet Phys.—JETP **14**, 1126 (1962)].
[13] A. Abragam and M. Borghini, *Progress in Low Temperature Physics* (North-Holland Publishing Company, Amsterdam, 1964), Vol. 4.

where

$$d_{\pm}=\pm\tfrac{3}{2}(g_{\perp}\beta M/r^3H)\sin\Theta\cos\Theta e^{\pm i\Phi},$$

and Θ, Φ are the spherical coordinates of $\mathbf{r}$ with respect to (x,y,z). This admixture allows one to induce the two so-called forbidden transitions $\Delta M=1$, $\Delta m=\pm1$, shown as W_2 and W_3 in Fig. 2, at the rate

$$W_2=W_3\approx(3/10)(g_{\perp}\beta/r^3H)^2W_1\equiv\sigma W_1\ \text{sec}^{-1}, \quad (3)$$

where we have used the spatial average $\langle\cos^2\Theta\sin^2\Theta\rangle=2/15$. These weak forbidden lines appear on either side of the main line at $H_0=h\nu_e/g_{\perp}\beta$, as shown schematically in Fig. 3(a). Typically, $\sigma\approx10^{-3}$ to 10^{-5}, and the satellites are actually only rarely observed.

Finally, an rf field H_{1n} at the proton resonance frequency $\nu_n=g_n\beta H/h$ will induce the nmr transitions $\Delta M=0$, $\Delta m=1$ at the rate

$$W_4=\tfrac{1}{2}T_{2n}(\gamma_nH_{1n})^2\ \text{sec}^{-1}, \quad (4)$$

which can be used to monitor the proton polarization with W_4 negligibly small.

The Nd ions and the protons are embedded in the crystal lattice, whose thermal vibrations induce relaxation transitions, shown schematically as w_1, w_2, w_3, and w_4 in Fig. 2. Viewing the entire crystal as a system of typical pairs, we can say that at thermal equilibrium the relaxation transitions establish relative populations given by the Boltzman factors in Fig. 2, column (a), where $\Delta\equiv h\nu_e/kT$, $\delta\equiv h\nu_n/kT$. In contrast to the oscillator induced transitions, which are equal for upward or downward transitions, the relaxation transitions are greater downward, and must be weighted by the Boltzman factor in the final state. This is essentially because the excitation number $[e^{h\nu/kT}-1]^{-1}$ of the phonons is many orders smaller than for the microwave photons, whose effective temperature $T>10^{10}$ °K, typically.

We associate the relaxation rate w_1 with the Nd^{3+} spin-lattice relaxation rate T_{1e}^{-1}, of order 10^2 to 10^5 sec^{-1} under our typical conditions.[14] This relaxation is due to the interaction of the electric multipole moments of the Nd ion with the thermally modulated crystal electric field gradients. In the effective spin Hamiltonian formalism, it is phenomenologically represented by a random time dependent perturbation $\mathcal{H}_T'\approx g\beta\mathbf{S}\cdot\mathbf{H}'(t)$ acting on the static wave functions $|M,m\rangle$, yielding a relaxation rate w_1 involving Nd^{3+} spin flips, as well as relaxation rates w_2 and w_3 involving simultaneous Nd^{3+}-proton spin flips. Since $\mathcal{H}_T'$ has the same form as the microwave perturbation $g\beta\mathbf{S}\cdot\mathbf{H}_1(t)$, we expect a relationsip similar to Eq. (3):

$$w_2=w_3\approx\sigma w_1. \quad (5)$$

The matrix elements $\langle M,\tfrac{1}{2}|\mathcal{H}_T'|M,-\tfrac{1}{2}\rangle$ vanish. The relaxation rate w_4 for proton flips unaccompanied by Nd^{3+} flips may arise from: thermal modulation of $\mathcal{H}_{dd}$, the Waller process; rotation of H_2O molecules; the $\mathcal{H}_T'$ perturbation in higher order. All these are negligible. Undesirable paramagnetic impurities, other than Nd^{3+}, will probably be the chief contributor to w_4, referred to as the "extraneous" proton relaxation rate. Ideally we expect $w_1\gg w_2=w_3\gg w_4$. It is worth noting that a different model of nuclear relaxation,[15] which assumes that the relaxation perturbation is the last term of Eq. (1) with $\mathbf{S}(t)$ a random time variable, does yield the result that $w_3\approx w_4$.

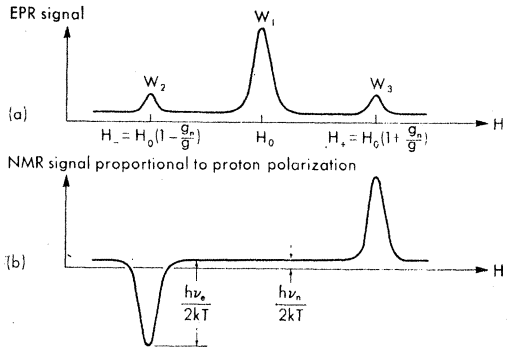

FIG. 3. (a) Paramagnetic resonance spectrum of Nd^{3+} ion, showing the main line W_1, flanked by two forbidden satellites W_2 and W_3. (b) Dynamic proton polarization induced at a fixed microwave frequency ν_e by varying the field through the forbidden transitions.

If we strongly induce, i.e., saturate, the forbidden transition W_3 with the microwave oscillator, the relative populations of the states $|\tfrac{1}{2},\tfrac{1}{2}\rangle$ and $|-\tfrac{1}{2},-\tfrac{1}{2}\rangle$ become equal to unity; the dominant w_1 relaxation will then bring the population of $|\tfrac{1}{2},-\tfrac{1}{2}\rangle$ to $e^{-\Delta}$ and that of $|-\tfrac{1}{2},\tfrac{1}{2}\rangle$ to e^{Δ}. The dynamic proton polarization from these drastically rearranged populations, Fig. 2, column (b), is given by

$$p_i=\frac{\bar{m}}{I}=\frac{n(m=\tfrac{1}{2})-n(m=-\tfrac{1}{2})}{n(m=\tfrac{1}{2})+n(m=-\tfrac{1}{2})}=\tanh\left(\frac{h\nu_e}{2kT}\right), \quad (6)$$

which is enhanced by a factor $\nu_e/\nu_n\sim10^3$ over the thermal equilibrium polarization $p_0=\tanh(h\nu_n/2kT)\approx h\nu_n/2kT$. Saturation of the other forbidden transition W_2 yields the populations of Fig. 2, column (c) and $p_i=-\tanh(h\nu_e/2kT)$; saturation of W_1 yields $p=p_0$, in column (d). This idealized over-all effect is shown in Fig. 3(b).

B. Average Shell-of-Influence Model

Turning now from the typical I, S pair to the whole crystal in which the protons greatly outnumber the Nd ions, we make the rough approximation that all the protons can be grouped into shells of influence about the ions, indicated schematically in Fig. 4. That is, all the protons $\mathbf{I}$ in the shell $r_1<r<r_2$ belong to the ion $\mathbf{S}$

[14] P. L. Scott and C. D. Jeffries, Phys. Rev. 127, 32 (1962).

[15] N. Bloembergen, Physica 15, 386 (1949); J. Hatton and B. V. Rollin, Proc. Roy. Soc. (London) A199, 222 (1949).

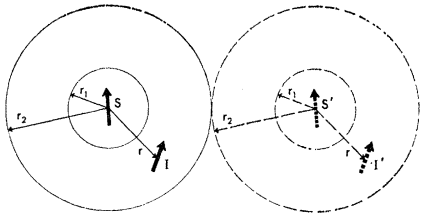

FIG. 4. All protons **I** within the shell-of-influence $r_1<r<r_2$ belong to the Nd^{3+} ion **S**; similarly the protons **I'** belong to the ion **S'**, etc.

at the center of this shell, in the sense that **S** is the source of their dynamic polarization and most of their relaxation. Here r_1 is the minimum distance between **S** and **I**; and r_2 is roughly half the average **S**—**S** spacing. We take $r_1=4.36$ Å from x-ray analysis of $Ce_2Mg_3(NO_3)_{12}\cdot 24H_2O$ ("CeMN"), which is isostructural with LaMN. We take $r_2\approx(4\pi N/3)^{-1/3}$, where N is the number of Nd ions per cc; for 1% Nd in LaMN, $N=1.6\times10^{19}$ and $r_2\approx 24$ Å.

We consider a single shell to be representative of the entire crystal, and so find rate equations for the average proton polarization in a shell. It is convenient to start with the separated energy levels of Fig. 5 for n_0 protons loosely coupled to a Nd ion at the center of the shell. Let N_1 be the probability to find the ion in state $M=\frac{1}{2}$, etc., so that the Nd polarization is given by

$$P=(N_1-N_2)/(N_1+N_2), \tag{7a}$$

with thermal equilibrium value

$$P_0=-\tanh(h\nu_e/2kT). \tag{7b}$$

The negative sign of P_0 comes from our implicit assumption that the ion magnetic moment is negative, but the final results for the dynamic proton polarization are independent of this assumption. Let $\bar{n}_1$ be the number of protons, averaged over the shell, in state $m=-\frac{1}{2}$, etc., so that the average proton polarization is

$$\bar{p}=(\bar{n}_2-\bar{n}_1)/(\bar{n}_2+\bar{n}_1), \tag{7c}$$

with the thermal equilibrium value

$$p_0=\tanh(h\nu_n/2kT). \tag{7d}$$

With reference to Fig. 2 we take w_1 for the ion-lattice relaxation rate, $\bar{w}_4$ for the average extraneous proton relaxation rate, and $\bar{w}_2=\bar{w}_3=\bar{\sigma}w_1$ for the average ion-proton simultaneous relaxation rate, where $\bar{\sigma}$ is obtained from Eq. (3) by taking the average of r^{-6} over the shell:

$$\langle r^{-6}\rangle=\int_{r_1}^{r_2} r^{-6}r^2dr\Big/\int_{r_1}^{r_2} r^2dr=r_1^{-3}r_2^{-3}.$$

Thus

$$\bar{\sigma}=\frac{3}{10}\left(\frac{g_1\beta}{H}\right)^2\frac{1}{r_1^3r_2^3}. \tag{8}$$

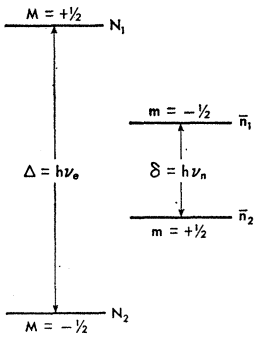

FIG. 5. Energy levels of protons, with shell average populations $\bar{n}_1$ and $\bar{n}_2$; energy levels of a Nd^{3+} ion with populations N_1 and N_2.

Similarly we take W_1, $\bar{W}_2=\bar{\sigma}W_1$, $\bar{W}_3=\bar{\sigma}W_1$, and W_4 as the oscillator-induced transition rates. The total rate of change of $\bar{n}_2$ is then (cf. Figs. 2 and 5)

$$\begin{aligned}d\bar{n}_2/dt=&\bar{w}_4[\bar{n}_1\exp(\delta/2)-\bar{n}_2\exp(-\delta/2)]\\&+W_4[\bar{n}_1-\bar{n}_2]+\bar{n}_1N_1\left[\bar{w}_2\exp\left(\frac{\Delta+\delta}{2}\right)+\frac{\bar{W}_2}{n_0}\right]\\&+\bar{n}_1N_2\left[\bar{w}_3\exp\left(\frac{(-\Delta+\delta)}{2}\right)+\frac{\bar{W}_3}{n_0}\right]\\&-\bar{n}_2N_1\left[\bar{w}_3\exp\left(\frac{\Delta-\delta}{2}\right)+\frac{\bar{W}_3}{n_0}\right]\\&-\bar{n}_2N_2\left[\bar{w}_2\exp\left(\frac{-\Delta-\delta}{2}\right)+\frac{\bar{W}_2}{n_0}\right].\end{aligned} \tag{9}$$

This equation differs from that used earlier[1] in two respects. We have used the exact form of the Boltzman factors to ensure validity when $h\nu_e/kT\gg1$. And we have retained the factor $1/n_0$ in the $\bar{W}_2$ and $\bar{W}_3$ terms, while omitting it in the $\bar{w}_2$ and $\bar{w}_3$ terms for the following reasons. The $\bar{W}_3$ transition is induced by a microwave photon of energy $h(\nu_e-\nu_n)$ just needed to flip simultaneously the ion and one proton; energy must be conserved, and in the absence of relaxation, this requirement is satisfied by the condition $n\Delta p=N\Delta P$, met by Eqs. (11) and (12). On the other hand, the $\bar{w}_3$ relaxation process can flip the ion and many protons simultaneously, since the lattice can absorb any amount of energy. This is admittedly an approximation but a better one than that used previously.

A similar rate equation for N_2 can be combined with Eq. (9) to yield effective rate equations for the average proton polarization $\bar{p}$ and the average Nd ion polarization P for the whole crystal, containing N Nd ions and n protons per cc:

$$\begin{aligned}d\bar{p}/dt=&-2W_4p-[(\bar{p}-p_0)/T_{1p}]-\bar{W}_2\frac{N}{n}(\bar{p}-P)\\&-\bar{W}_3\frac{N}{n}(\bar{p}+P),\end{aligned} \tag{10}$$

$$\begin{aligned}dP/dt=&-2W_1P-[(P-P_0)/T_{1e}]-\bar{W}_2(P-\bar{p})\\&-\bar{W}_3(P+\bar{p}),\end{aligned} \tag{11}$$

where

$$1/T_{1e}=2w_1(1+\bar{\sigma})\cosh(\Delta/2)\approx 2w_1\cosh(\Delta/2), \quad (12)$$

$$1/T_{1p}=2\bar{w}_4+\bar{\sigma}(1-PP_0)/T_{1e}. \quad (13)$$

Looking at Eq. (11) with $W_1=\bar{W}_2=\bar{W}_3=0$, we see that $P\rightarrow P_0$ exponentially at the rate T_{1e}^{-1}, which we identify as the Nd ion-lattice relaxation rate. Similarly, in the absence of induced transitions, $p\rightarrow p_0$ exponentially at the rate T_{1p}^{-1}, which we identify as the average proton relaxation rate, due to the Nd ions and to extraneous impurities. By neglecting the latter [i.e., taking $\bar{w}_4\approx 0$ in Eq. (13)], taking $\bar{\sigma}$ from Eq. (8), and $P=P_0$, we see that the shell-of-influence model predicts

$$\frac{1}{T_{1p}}\approx\frac{3}{10}\left(\frac{g_1\beta}{H}\right)^2\frac{1}{r_1^3r_2^3}\frac{1}{T_{1e}}\operatorname{sech}^2\left(\frac{h\nu_e}{2kT}\right) \quad (14)$$

for the relationship between T_{1p} and T_{1e}.

For large Nd^{3+} polarizations, the last factor in Eq. (14) is approximately proportional to the probability of the ion being in the $M=+\frac{1}{2}$ state; it has its physical origin as follows: for $(h\nu_e/kT)\gg 1$ only the ion state $M=-\frac{1}{2}$ in Fig. 5 will be significantly populated. Except for the $\bar{w}_4$ relaxation, assumed negligible, a proton can flip down from $m=-\frac{1}{2}$ to $m=+\frac{1}{2}$ by a simultaneous ion flip from $M=+\frac{1}{2}$ to $M=-\frac{1}{2}$; but there are exceedingly few ions with $M=+\frac{1}{2}$. Or the proton can flip down by a simultaneous ion flip from $M=-\frac{1}{2}$ to $M=+\frac{1}{2}$; but there are exceedingly few lattice phonons to supply this energy. As $T\rightarrow 0$, even though T_{1e}^{-1} becomes a finite constant because of spontaneous phonon emission, Eq. (14) predicts that $T_{1p}^{-1}\rightarrow 0$ as $\operatorname{sech}^2(h\nu_e/2kT)$. The consequence of this is that the proton relaxation time should become extremely long, $\sim$ days, at accessible frequencies and temperatures, say $\nu_e=75$ kMc/sec and $T=0.3$°K, provided that the relaxation $\bar{w}_4$ can be made negligible.

To find the dynamic proton polarization we take the steady state solutions of Eqs. (10) and (11), assuming that only transition $\bar{W}_3$ is induced, obtaining $P_{ss}\approx P_0=-\tanh(h\nu_e/2kT)$, and

$$\bar{p}_{ss}\approx\frac{T_{1e}\bar{W}_3\tanh(h\nu_e/2kT)}{\bar{f}+T_{1e}\bar{W}_3(1+\bar{f})}, \quad (15a)$$

where we have introduced the sample average leakage factor

$$\bar{f}=(n/N)(T_{1e}/T_{1p}). \quad (15b)$$

Writing $\bar{W}_3=\bar{\sigma}s/2T_{1e}$, where

$$s=T_{1e}T_{2e}(\gamma_eH_{1e})^2 \quad (16)$$

is the usual epr saturation factor, we rewrite Eq. (15) as

$$\bar{p}_{ss}\approx\left[\frac{\tanh(h\nu_e/2kT)}{1+\bar{f}}\right]\left(\frac{s}{s+s_{1/2}}\right), \quad (17a)$$

$$s_{1/2}=2f/(1+\bar{f})\bar{\sigma}. \quad (17b)$$

The term in brackets gives the maximum polarization $\bar{p}_{\max}$ at complete saturation; the second factor shows the dependence on $s\propto(H_{1e})^2$, i.e., on the average squared microwave field in the crystal.

For the ideal case $\bar{w}_4=0$, we find $\bar{f}=(n/N)\bar{\sigma}\operatorname{sech}^2\times(h\nu_e/2kT)$. For the typical case of 1% Nd in LaMN at $\nu_e=75$ kMc/sec, $T=1.5$°K we have, $\bar{\sigma}\sim 10^{-6}$, $(n/N)\sim 2\times 10^3$, $\bar{f}\sim 10^{-3}$, and thus

$$s_{1/2}\approx(2n/N)\operatorname{sech}^2(h\nu_e/2kT), \quad (18a)$$

which is of order 10^3 for our typical case. In comparison to the main epr resonance which becomes half saturated at $s=1$, Eq. (18a) predicts that much larger microwave fields are required to half saturate the dynamic polarization. This arises in the following way: in the steady state the number of protons flipping down by relaxation is $\sim n/T_{1p}$ sec^{-1}; this must equal the number $N\bar{W}_3$ sec^{-1} flipped up by the forbidden transition acting only on N Nd ions, where $N\ll n$. This argument also yields Eq. (18a). It should be noted that this prediction and the discussion in the following paragraph is based on the assumption that the ion directly flips all the protons through the average dipolar interaction in the shell. Although free spin diffusion does not seem to enter significantly in the proton relaxation because of the diffusion barrier, as discussed in Sec. IV C, this barrier may be partially broken down by the microwave fields, thus reducing the required saturation factor considerably below Eq. (18a); this is indicated in the experimental results, Sec. IV, 4.

We estimate the actual microwave power required by adding the power absorbed by the crystal sample to that lost in the cavity walls. In the ideal case of saturation of a well resolved forbidden transition the power absorbed by the sample is

$$P_s\approx\bar{W}_3Nh\nu_e\approx nh\nu_eT_{1p}^{-1}\text{ ergs cm}^{-3}\text{ sec}^{-1}, \quad (18b)$$

which has the typical value $P_s\approx 1$ mW at 70 kMc/sec and $T_{1p}^{-1}=6\times 10^{-4}$ sec^{-1}. In a large random mode cavity of volume V and quality factor Q when empty [define $Q=2\pi\nu_e\times$average energy stored$\div$energy lost per sec], it can be shown that $\frac{1}{4}\langle H_{1y}^2\rangle_{\text{av}}=\langle(H_{1e})^2\rangle_{\text{av}}=\frac{2}{3}PQ/V\nu_e$. From Eqs. (2b), (16), and (18b) we obtain

$$P_c\approx\frac{(3/4)sH_{1/2}V\nu_e}{T_{1e}\gamma_eQ}\times 10^{-7}\text{ W} \quad (18c)$$

for the power lost in the cavity walls. For the typical values $H_{1/2}=$epr linewidth at half-maximum$=6$ Oe, $V=1$ cc, $\nu_e=70$ kMc/sec, $T_{1e}=10^{-4}$ sec, $\gamma_e=2.3\times 10^7$ (Oe sec)$^{-1}$, $Q=10^4$, we find $P_c\sim 1.3\,s$ mW. Thus for $s\sim 10^3$, required by Eq. (18a) for half saturation of the dynamic polarization, the cavity wall losses may greatly exceed the sample losses.

For comparison we calculate similarly the power absorbed by the sample in saturation of the main epr

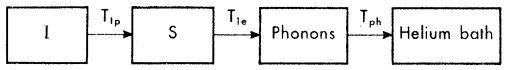

FIG. 6. Thermal block diagram of protons I, Nd^{3+} ions S, crystal lattice phonons, and liquid helium bath. T_{1p} is the proton-ion relaxation time, T_{1e} is the ion-phonon relaxation time, T_{ph} is the phonon-bath relaxation time.

line

$$P_s' \approx W_1 N h\nu_e \approx N h\nu_e / T_{1e}^{-1} \text{ erg cm}^{-3} \text{ sec}^{-1}, \quad (18d)$$

which has the typical value ~ 7 W for $N=1.6\times10^{19}$, $\nu_e=70$ kMc/sec and $T_{1e}=10^{-4}$ sec, appropriate for 1% Nd in LaMN. The cavity losses will be given by Eq. (18c) with $s=1$, which has the value ~ 1 mW typically. These results imply that most of the microwave power goes into the sample in saturating the main epr line, in contrast to the forbidden line, where most power goes into the cavity walls.

If the sample is not in good thermal contact with the helium bath the absorbed power may heat it and thus shorten T_{1e}, which can have a strong exponential temperature dependence in the Orbach relaxation region (see Sec. IV A). Since the power absorbed is proportional to T_{1e}^{-1}, even more absorption and more heating, etc., occur in a runaway process in which the temperature of the crystal quickly jumps well above the helium bath, accompanied by a disappearance of the dynamic polarization.

It is known[14,16] that the Nd^{3+} ion-lattice direct relaxation is phonon bottlenecked at the high fields used in dynamic polarization. Consider the thermal block diagram of Fig. 6. Energy flows from the hot proton spins I to the ions S at the rate $nh\nu_e T_{1p}^{-1} \sim 10^4$ erg cm^{-3} sec^{-1}, typically. Energy flows from the ions to lattice phonons at the rate $E_{ez}/T_{1e} \approx N h\nu_e T_{1e}^{-1} \sim 10^7$ erg cm^{-3} sec^{-1}, typically. The phonon energy flows to the helium bath at the rate $E_{ph}/T_{ph} \sim 10^6$ erg cm^{-3} sec^{-1}, typically using $E_{ph}=12\pi\nu_e^2\Delta\nu h\nu_e/v^3$ for the phonon energy and $T_{ph}=(v/\text{crystal thickness}) \approx 10^{-7}$ sec for the phonon relaxation time. It is clear that the $I \rightarrow S$ rate is orders of magnitude smaller than the others and thus will limit the transport of excess proton Zeeman energy to the bath. The proton relaxation will not be bottlenecked; we should use for T_{1e} in Eq. (14) and true Nd^{3+} spin-lattice relaxation rate. In the above example since $E_{ez}T_{1e}^{-1} > E_{ph}T_{ph}^{-1}$, one does not actually observe T_{1e} in the usual type of pulse-recovery experiment to measure the ion-lattice relaxation time, but rather the longer bottlenecked time $T_b = T_{ph}E_{ez}/E_{ph} \propto T^{-2}$.[14] This effect makes the epr resonance easier to saturate and somewhat modifies the microwave power estimates in the preceding paragraph.

Although the rate equations (10) and (11) are not linear because of the dependence of T_{1p} on P in (13), saturation of $\bar{W}_3$ does not disturb P very much from its thermal equilibrium value P_0. The coupled linearized equations can be solved for the two time constants τ_1 and τ_2, which, for $n \gg N$, are

$$\frac{1}{\tau_1} = \frac{1}{T_{1p}}\left(1+\frac{s}{s_{1/2}}\right), \quad (19a)$$

$$\frac{1}{\tau_2} = \frac{1}{T_{1e}}\left(1+\frac{\bar{\sigma}s}{2}\right), \quad (19b)$$

with $s_{1/2}$ given by Eq. (18a). The time constant τ_1 can be associated with the build up of the dynamic polarization. From Eqs. (17) and (19a) we further obtain $\tau_1 \approx T_{1p}(1-\bar{p}/\bar{p}_{\max})$.

C. Local Fields

Actually the total magnetic field that a given proton or ion feels is the applied field $\mathbf{H}$ plus the sum of the dipole fields of all the other magnetic dipoles in the crystal, e.g., other Nd ions, protons, N^{14} nuclei, etc. At a given lattice site the remote dipoles contribute an average field expressible in terms of the macroscopic magnetization $\mathbf{M}$ and the sample shape. The nearby dipoles contribute a distinct field dependent on the crystal structure, which may give rise to a structure in the magnetic resonance lines. Finally, the probability that the neighboring dipoles can be pointing either up or down gives a random distribution of local fields over the whole crystal and hence a finite linewidth.

Since we are particularly interested in proton linewidths, shifts, and structures arising at high polarizations, we look first at the local field in pure LaMN at the proton sites. If the crystal has ellipsoidal shape we can use the classical expression for the local field $\mathbf{H}_{li}$ at the ith proton site due to all the other protons

$$\mathbf{H}_{li} = \mathbf{H} + [(4\pi/3) - N']\mathbf{M} + \sum_j \mathbf{H}_{ij}, \quad (20)$$

where N' is the sample demagnetization factor and $\mathbf{H}_{ij}$ is the dipole field at the ith site due to the jth proton. The $\sum_j$ is over a small Lorentz sphere, and vanishes if the protons are arrayed in cubic symmetry, which is not the present case.

Assuming that $\mathbf{M}$ is due only to protons, we take $\mathbf{M} \| \mathbf{H}$ with $M = n g_n \beta \bar{p}/2$, which has the saturation value $M_{0p}=0.53$ Oe in LaMN when $\bar{p} \rightarrow 1$; this term shifts the local field by ~ 2 Oe at complete polarization. Since there are a large number of proton sites in a unit cell, we expect that the sum $\sum_j \mathbf{H}_{ij}$ may have a different value for each site, thus giving a series of proton resonance lines. If we assume that all proton spins are parallel to $H \| z$, i.e., $\bar{p}=1$, then the z component of this sum becomes

$$H_i = 14.1 \sum [(3\cos^2\Theta_{ij} - 1)/r_{ij}^3] \text{ Oe}, \quad (21)$$

where $\mathbf{r}_{ij}$ (in Å) is the distance between $\mathbf{I}_i$ and $\mathbf{I}_j$, and $\Theta_{ij} = \angle \mathbf{H}, \mathbf{r}_{ij}$. This sum has been evaluated[17] with an

[16] J. M. Baker and N. Ford, Phys. Rev. 136, A1692 (1964).

[17] We are indebted to Dr. N. Ford for making this calculation.

IBM 7090 computer using x-ray structure data for CeMN[18] for the approximately 500 protons with $r_{ij}<15$ Å. Since CeMN and LaMN are isostructural, we will assume that this sum, and the others below, are essentially correct for LaMN. The calculations were made for the two crystal orientations (cf. Fig. 10) (a) $\theta=90°$, $\varphi=30°$, 90°, $\cdots$; (b) $\theta=90°$, $\varphi=0°$, 60°, $\cdots$. In each case H_i was found to have 24 distinct values spread over about 20 Oe. If the proton frequency is fixed at $\nu_n=g_n\beta H_0/h$, and resonance is observed by varying H, one expects for the proton spectrum a series of sharp lines at the fields

$$H_{ri}=H_0-[(4\pi/3)-N']M-H_i, \qquad (22)$$

as indicated in Fig. 7. For complete negative polarization, $\bar{p}=-1$, the spectrum would be reflected through the line $H_i=0$. Since there is no randomness in proton orientation, there is no linewidth arising from the dipolar fields of other protons. If other sources of linewidth (e.g., that due to nonoriented N^{14} nuclei) can be made negligible, this opens the possibility of high-resolution nmr spectroscopy in solids, and the investigation of such interactions as pseudonuclear exchange $J\mathbf{I}_1\cdot\mathbf{I}_2$, etc.

Starting with the spectrum of Fig. 7 for complete proton polarization we ask what happens as the polarization is decreased. The lines will broaden and also shift as $\bar{p}$ is reduced. At $\bar{p}\ll1$, the spectrum can be approximately described: the protons in each H_2O molecule will show two equal resonance lines, spaced by $(3g_n\beta/4)(3\cos^2\Theta-1)/r^3$, analogous to the spectrum seen in $CaSO_4\cdot 2H_2O$ [19]; these 24 pairs of lines can be roughly obtained by adding the spectrum of Fig. 7 and its mirror image and multiplying by 3/2. However each line will now have a sizable linewidth which washes out most, but not all, of the structure. The observed proton nmr lines at $\bar{p}\ll1$ are quite different for the two orientations $\varphi=0$ and $\varphi=30°$ [cf., Fig. 21 and Fig. 22a] and bear out the above expectations. To summarize, the broad symmetric line shape at low polarizations changes over to an asymmetric line at high polarizations, eventually becoming resolved into many sharp lines at 100% polarization.

The expression of Van Vleck[20] for the root of the second moment of a proton line is

$$\Delta H_{\rm rms})_{T=\infty}=[\langle\Delta H^2\rangle]^{1/2}=\frac{3}{2}\cdot\frac{g_n\beta}{2}\left\{\sum_j\left[\frac{3\cos^2\Theta_{ij}-1}{r_{ij}^3}\right]^2\right\}^{1/2}, \qquad (23)$$

due to all the other protons, assumed to be "alike"; the factor 3/2 is removed if they are unalike, i.e., have resolvably different resonance frequencies. Equation

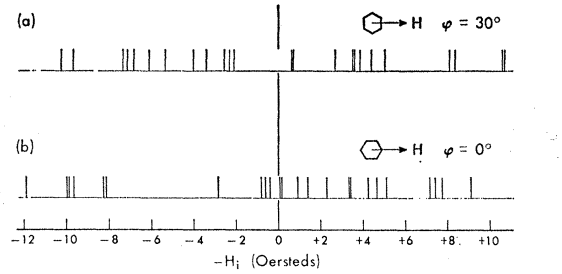

FIG. 7. The fields $-H_i$ calculated from Eq. (21) for the 24 proton sites in LaMN for the orientations (cf. Fig. 10) (a) $\theta=90°$, $\varphi=30°$, 90°, $\cdots$; (b) $\theta=90°$, $\varphi=0$, 60°, $\cdots$. The figures represent the expected proton resonance spectrum at complete positive polarization as the field is increased from left to right.

(23) has been evaluated for LaMN by summing over all protons within 15 Å about each different proton site. At $\theta=90°$, $\varphi=0$ the average value for all sites is $\Delta H_{\rm rms})_{T=\infty}\approx9.1$ Oe, although there is a considerable variation from site to site. We have similarly evaluated the contribution to the proton rms linewidth due to La^{139}, N^{14}, and Mg^{25}, obtaining 0.09, 0.07, and 0.05 Oe, respectively.

Equation (23) was derived under the assumption that $\bar{p}\ll1$, i.e., that the temperature T is infinite. The calculation has been extended[21,22] to the general case where the polarization is not negligible, with the result

$$\Delta H_{\rm rms})_T=\Delta H_{\rm rms})_{T=\infty}[1-\bar{p}^2]^{1/2}. \qquad (24)$$

If we use for $\bar{p}$ the ideal dynamic value p_i of Eq. (6), the proton rms linewidth becomes

$$\Delta H_{\rm rms})_T-\Delta H)_{{\rm rms}T=\infty}\,\mathrm{sech}(h\nu_e/2kT). \qquad (25)$$

For $\nu_e/T=150$ kMc/sec/°K, we calculate $p_i=0.998$ and $\mathrm{sech}(h\nu_e/2kT)\approx0.05$, corresponding to a very considerable reduction in linewidth, sufficient to resolve the spectrum of Fig. 7. However, the lines widen appreciably as $\bar{p}$ decreases slightly, and in the actual experiments where $\bar{p}\approx0.7$ the structure is only poorly resolved at best. Its resolution would be a simple indicator of essentially complete polarization.

Although we have been neglecting the dipole field $H_{\rm Nd}$ of the Nd ion on the protons, this is appreciable for the near protons: at $r=10$ Å, $H_{\rm Nd}\sim g_1\beta/2r^3\sim12$ Oe; at $r=20$ Å, $H_{\rm Nd}\sim1$ Oe. Since $T_{1e}\gg T_{2n}$, the field $H_{\rm Nd}$ is essentially static; it significantly lowers the resonance field for protons at $r<7$ Å, so that their resonance is probably not observed. The saturation magnetization of 1% Nd^{3+} in LaMN is $M_{0N}=0.2$ Oe, comparable to M_{0p}, and should be included in M in Eqs. (20) and (22).

Next we estimate the local magnetic field at the Nd ions, which for concentrations smaller than 1% is due chiefly to the protons. For $\bar{p}=1$, Eq. (21) has been evaluated at the Nd site (they are all equivalent) due

[18] A. Zalkin, J. D. Forrester, and D. H. Templeton, J. Chem. Phys. **39**, 288 (1963).
[19] G. E. Pake, J. Chem. Phys. **16**, 327 (1948).
[20] J. H. Van Vleck, Phys. Rev. **74**, 1168 (1948).
[21] K. Kambe and T. Usui, Progr. Theoret. Phys. (Kyoto) **8**, 302 (1952).
[22] M. McMillan and W. Opechowski, Can. J. Phys. **38**, 1168 (1960).

to all the 561 protons within $r_{ij}=15$ Å. This calculation[17] was made with a computer using x-ray structure data of CeMN. The results are: $H_{i0}=-0.476$ Oe for $\theta=0$; $H_{i0}=+0.237$ Oe for $\theta=90°$, $\varphi=0$ or 90°. For less than complete polarization we assume that H_i is just proportional to $\bar{p}$, and write an equation

$$H_0-H_{\rm res}=\{[(4\pi/3)-N']M_{0p}+H_{i0}\}\bar{p} \qquad (26)$$

for the shift of the Nd^{3+} resonance field as a function of the proton polarization $\bar{p}$. For a thin LaMN crystal with H in the plane, $H_{i0}=+0.237$ Oe, and the shift is 2.42 $\bar{p}$ Oe, a significant amount, comparable to the Nd resonance linewidth. This means that in order to remain on true forbidden resonance the applied field must be slightly readjusted as the dynamic polarization builds up. Equation (26) can also be used to calculate $\bar{p}$ from the measured shift of the La^{139} nuclear magnetic resonance.

The Van Vleck expression, Eq. (23), for the Nd epr linewidth in LaMN due to all the protons within $r_{ij}=15$ Å has also been calculated[17] with these results for crystal orientation $\varphi=0$: $\Delta H_{\rm rms}=0.80$ Oe for $\theta=90°$; $\Delta H_{\rm rms}=0.61$ Oe for $\theta=45°$; and $\Delta H_{\rm rms}=0.84$ Oe for $\theta=0°$. Similar calculations of the linewidth due to N^{14} nuclei gave the small values 0.7×10^{-2} Oe, 0.6×10^{-1} Oe, and 0.3×10^{-1} Oe at the corresponding angles. Assuming a Gaussian line shape, we thus predict a Nd linewidth $H_{1/2}=2\Delta H_{\rm rms}=1.6$ Oe between points of maximum slope for $z'\perp H$, due to the protons alone. This is close to the peak-to-peak derivative linewidth component 1.4 Oe observed by Scott, Stapleton, and Wainstein,[23] who find additional contributions to the linewidth due to small random fluctuations in the g tensor. However, in contrast to Ce^{3+}, the Nd^{3+} epr lines are found to be relatively sharp, $H_{1/2}\approx6$ Oe at $H=20$ kOe, and do not seem to depend on crystal size. This was an important factor in our determination to make detailed studies of dynamic polarization in Nd, LaMN at high fields.

III. APPARATUS AND CRYSTALS

A. Magnetic Resonance Apparatus

The basic arrangement used, Fig. 1, is simply a tunable cavity coupled to a microwave oscillator at ν_e, used to induce the forbidden transitions which polarize the protons. The polarization is simultaneously measured by the proton nmr absorption, observed by the change in the Q and hence in the rf voltage V across the coil wound around the crystal. A detailed block diagram is shown in Fig. 8, and the cavity-coil arrangement in Fig. 9.

Three different microwave oscillators were used: An Elliott type 8FK1 fixed-frequency klystron at 35 kMc/sec, with power output of 10 W; an OKI type 50V10 tunable klystron at 50 kMc/sec, with 50 mW power output; an Elliott type 4FK1 fixed frequency klystron at 74 kMc/sec, with power output up to 100 mW. One of these was coupled via an isolator, a calibrated attenuator, and a waveguide shutter switch to a thin-wall bronze RG96U waveguide leading to the cavity. A directional coupler sampled 1% of the reflected power, enabling observation of the allowed Nd^{3+} epr resonance line. The forbidden lines were usually too weak to be observed directly.

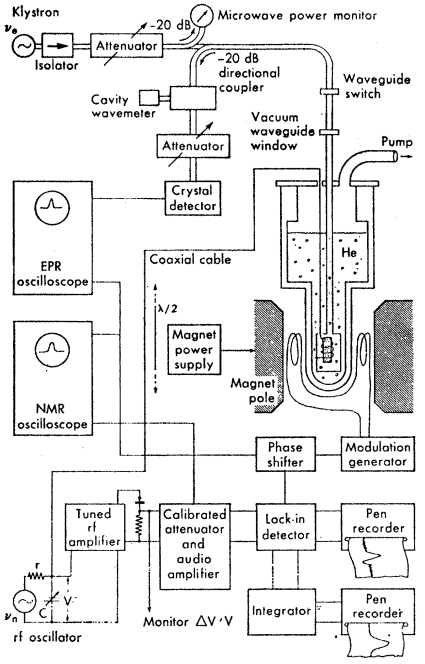

FIG. 8. Block diagram of dynamic proton polarization apparatus used at Berkeley.

The cavity, Fig. 9, is a brass cylinder with a tunable end plunger, spring loaded with Teflon to prevent microphonics. A large number of modes, particularly TE_{0nm} modes, are resonant over the range 35 to 75 kMc/sec. At the highest frequencies the modes are so closely spaced as to be nearly continuous, so that exact cavity tuning is not necessary. In fact our attempt has been to operate with several nearly degenerate modes, so that overlapping standing waves fill the entire cavity. This is essential in order to induce the forbidden transitions uniformly throughout the crystal, which may be large compared to the wavelength of the microwaves. Although a multimode cavity is suitable for dynamic polarization of large samples, it is unsatisfactory for epr spectroscopy: One usually observes a number of spurious resonances in the vicinity of the true epr resonance; these are probably due to frequency pulling of the modes by the paramagnetic dispersion of the sample.

The cavity is immersed in and filled with liquid He^4 in a metal Dewar, installed in a Berkeley 12 in. electromagnet with pole tips tapered to 4 in. diameter and $1\frac{5}{8}$ in. gap. With this arrangement we could operate at

[23] P. L. Scott, H. J. Stapleton, and C. Wainstein, Phys. Rev. 137, A71 (1965).

fields up to 22 kOe and temperatures in the range $1.3<T<4.2$°K by pumping on the helium with a mechanical pump (15 ft³/min). The temperature was determined from the He vapor pressure. The microwave power delivered to the cavity was calibrated from the incremental He boil-off rate at 4.2°K.

The crystal was mounted in the cavity between two flat loops of 40 gauge bare copper wire, which formed the rf coil; it was connected via a coaxial cable of length $\lambda/2$ to an external capacitance C, this parallel resonance circuit being driven with constant current by a Marconi model 1066B/1 signal generator through a high resistance r. It can be shown[3] that the fractional change in voltage $\Delta V/V$ at proton resonance is simply proportional to the proton polarization $\bar{p}$, provided $(\Delta V/V)\ll 1$. The derivative of the nmr absorption was recorded by using a small modulation field, a calibrated attenuator, a lock-in detector, and a pen recorder. Although small polarizations can be compared using the peak-to-peak height of the derivative signal, larger polarizations are accompanied by the line shape changes discussed in Sec. II C. An electronic integrator[24] was then used to directly integrate the derivative signal and record the true absorption curve on a paper tape. The area A under the absorption curve was obtained by cutting out the paper area and weighing it. At high polarizations the nmr absorption was so great that the detector linearity condition $(\Delta V/V)\ll 1$ was not always met; corrections were made as discussed in Sec. V.

B. Crystals

The LaMN crystal is isostructural with CeMN, whose structure has been accurately determined[18] by x-ray diffraction, using least-squares refinement, which locates most atoms to within $\sim 10^{-3}$ Å. Since the H atoms scatter x rays only slightly, their position is uncertain by ~ 0.3 Å; this uncertainty should be taken into account in using the proton dipole sums calculated in Sec. II C. The crystal is rhombohedral, space group $R\bar{3}$. All Ce^{3+} sites are magnetically equivalent; each Ce^{3+} is surrounded by twelve O atoms at an average distance 2.64 Å. The O atoms belong to six NO_3 ions at the corners of a somewhat irregular icosohedron. Each Mg atom is surrounded by six H_2O molecules, with the O atoms at the corners of an octahedron, with an average Mg-O spacing of 2.07 Å. One-fourth of the H_2O molecules are not coordinated to cations. The minimum Ce-H distance is 4.36 Å. The density is 2.1 g cm^{-3}, corresponding to 3.8×10^{22} protons/cm³ and 1.6×10^{21} Ce^{3+} ions/cm³. We assume that all these data apply also to LaMN, lightly doped with Nd^{3+}.

TABLE I. $(Nd,La)_2Mg_3(NO_3)_{12}\cdot 24H_2O$ crystals used in experiments.

Crystal number	Concentration of Nd	Chemical source La	Nd	Mg
1	1% enriched	a	c	f
2	1% enriched	a	c	f
5	1% natural	a	d	f
6	1% natural	a	d	f
11	1% enriched	a	c	f
12	1% enriched	a	c	f
13	1% natural	b	e	g

[a] $La(NO_3)_3\cdot 6H_2O$, Lindsay Chemical Company, Code 549. La~99.997%; Pr~0.001%; Fe~10^{-4}%.
[b] $La(NO_3)_3\cdot 6H_2O$, Lindsay Chemical Company, Code 549.9; La~99.999%.
[c] Nd_2O_3, Oak Ridge National Laboratory, series JI, lot 1119(a); enriched to 98.5% in even-even Nd isotopes.
[d] $Nd(NO_3)_3\cdot 6H_2O$, Lindsay Chemical Company, Code 659.9; Nd~99.9%; Pr~0.04%.
[e] $Nd(NO_3)_3\cdot 6H_2O$, Lindsay Chemical Company, Code 659.92; Nd~99.999%.
[f] $Mg(NO_3)_2\cdot 6H_2O$, Mallinckrodt analytical reagent; Fe~0.0005%.
[g] MgO, Johnson Mathey, Ltd., Catalog No. JM 130; Fe~0.0002%.

[24] We are indebted to Kenneth Langley for construction of this integrator.

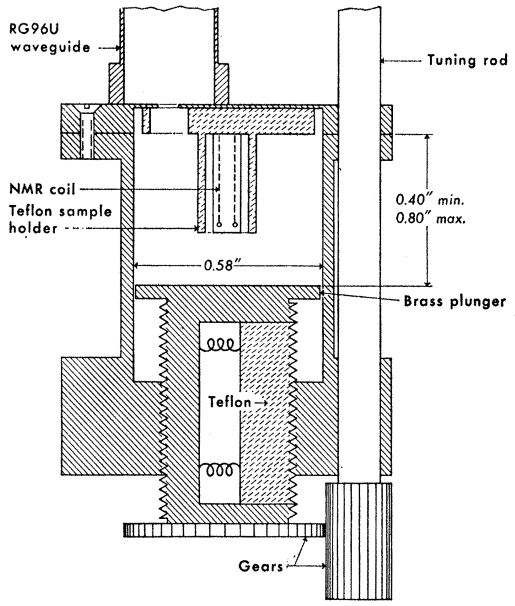

FIG. 9. Tunable high-mode microwave cavity and nmr resonance coil.

Many Nd, LaMN crystals were grown, some of which are listed in Table I. The concentration of Nd is that for the growing solution, prepared from stoichiometric amounts of Nd, La, and Mg nitrates. Since the proton relaxation time and polarization may depend somewhat on impurities, the sources of chemicals are listed along with the estimated impurities. The crystals were grown from saturated aqueous solution in a desiccator at 0°C. The actual concentration of Nd in the crystal may be less by a small variable factor from that of the solution, since the solubility of the Nd and La salts differ by ~10%. The crystals grow in flat hexagonal plates with the c (i.e., z') axis perpendicular to the plate, as shown in Fig. 10(a), which defines crystal axes (x',y',z') and the angles θ and φ. Figure 10(b) is an infrequent variant growth habit. The crystals in Table I were ~8 mm in diameter and ~1.5 mm thick, weighing 150 to 250 mg; they grew in ~24 h.

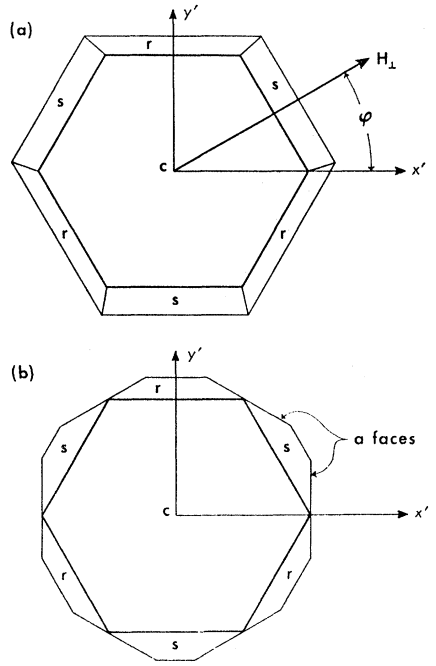

FIG. 10. (a) Common growth habit of $La_2Mg_3(NO_3)12\cdot 24H_2O$; (b) another growth habit. The crystal axes x', y', z' are defined as shown, with z' out of the paper. The H field direction is defined by φ and $\theta = \angle z', H$.

Natural Nd consists of 80% even-even isotopes for which there is no hyperfine structure (hfs); the Nd^{3+} allowed epr spectrum is a single line W_1. The odd isotopes 143 and 145 each show an epr spectrum of 8 hfs lines spread over ~1500 Oe. Although the nearest hfs line is ~60 Oe from the central line and does not overlap the forbidden line for the fields used, nevertheless the hfs lines act as sources of extraneous proton relaxation, and so we used Nd enriched in even isotopes in some crystals in Table I.

IV. PROTON RELAXATION IN $(Nd,La)_2Mg_3(NO_3)_{12}\cdot 24H_2O$

We have made detailed measurements of the proton relaxation time T_{1p} in several crystals of 1% Nd in LaMN over the field range $0.3<H\lesssim 20$ kOe and temperature range $1.3<T<4.2$°K. The data can only be understood in terms of the Nd^{3+} relaxation, which we first discuss.

A. Nd^{3+} Relaxation

The relaxation of Nd^{3+} in LaMN has been previously studied[14,16,25] and is well understood. The experimental results for $\theta=90°$ are

$$T_{1e}^{-1})_{Nd}=3\times10^{-18}H^5\coth(h\nu_e/2kT)+6\times10^9\exp(-47/T)\ \text{sec}^{-1}, \quad (27)$$

where H is in Oe. The first term (taken from the measurements of Baker and Ford[16] for a crystal from the same batch as crystal No. 12, Table I) represents the direct process in which a Nd ion flips from $M=+\frac{1}{2}$ to $M=-\frac{1}{2}$, giving up its energy to a lattice phonon of the same frequency. The H^5 field dependence and the temperature dependence in Eq. (27) are theoretically expected and experimentally verified; even the constant 3×10^{-18} is in good agreement with theoretical expectations. The second term (taken from our measurements on crystal No. 12, Table I) represents the Orbach process, in which an ion flips from $M=+\frac{1}{2}$ up to a crystal field excited state at $\Delta'=47$°K, and then down to $M=-\frac{1}{2}$, absorbing and emitting two phonons of energy $k\Delta'\pm h\nu_e/2$ in cascade. This process is approximately independent of field, but has a rapid exponential temperature dependence; again the constant 6×10^9 is in moderate agreement with theory. A term $T_{1e}^{-1}\propto T^9$ from the higher order Raman process is also expected, but is too small to be important here.

Anticipating an impurity of praseodymium in our crystals we take for the relaxation rate of Pr^{3+} in LaMN[14]

$$T_{1e}^{-1})_{Pr}=9\times10^{-7}\cos^3\theta H^3\coth(h\nu_e/2kT)+4.6\times10^{10}\exp(-54/T)+2.3T^7\ \text{sec}^{-1}, \quad (28)$$

where H is in Oe. The first term is the theoretical estimate of the direct process, which is so strong as to be severely bottlenecked, preventing its direct observation; the other terms are the measured Orbach and Raman processes. Since Pr^{3+} is a non-Kramers' doublet, there are direct matrix elements of the fluctuating crystal field between the doublet states, resulting in a strong direct process proportional to H^3. In a Kramers' doublet such as Nd^{3+} the matrix elements vanish except for admixtures to higher states through the Zeeman perturbation; the relaxation rate is reduced by the factor $\sim(g\beta H/k\Delta')^2$. Thus even small amounts of Pr^{3+} or other non-Kramers' doublets, e.g., Fe^{2+}, could have important contributions to the proton relaxation at the lowest temperatures; we expect relaxation due to these to be distinguishable from that due to Nd^{3+} by the different field dependence.

B. Measurements and Interpretation

The crystals used, Nos. 2, 5, and 12, Table I, each contained nominally 1% Nd^{3+}. For this case we evaluate Eq. (8), using $r_1=4.4$ Å, $r_2=24$ Å, $g_\perp=2.70$ to find $\bar{\sigma}=160/H^2$, where H is in Oe. Thus from Eqs. (14) and (27) we predict that the proton relaxation rate at $\theta=90°$ due to Nd^{3+} alone would be

$$\left(\frac{1}{T_{1p}}\right)_{Nd}=\left[4.8\times10^{-16}H^3\coth\left(\frac{g_\perp\beta H}{2kT}\right)+\frac{9.6\times10^{11}}{H^2}\exp\left(\frac{-47}{T}\right)\right]\text{sech}^2\left(\frac{g_\perp\beta H}{2kT}\right)\text{sec}^{-1}. \quad (29)$$

[25] R. H. Ruby, H. Benoit, and C. D. Jeffries, Phys. Rev. **127**, 51 (1962).

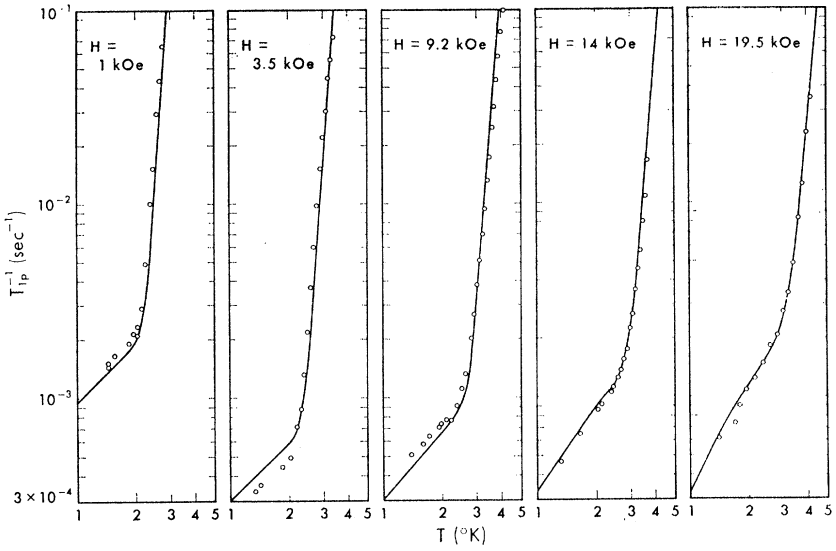

FIG. 11. Observed proton relaxation rate T_{1p}^{-1} versus temperature T for 1% Nd in LaMN (crystal No. 12, Table I), oriented with $\theta=90°$, $\varphi=0°$. The solid curves are given by Eq. (30).

The relaxation time T_{1p} was measured by first dynamically polarizing the protons to an enhancement $E\sim100$. The microwaves were then turned off and the proton nmr derivative peak-to-peak signal $S(t)$ sampled periodically as it decayed to its thermal equilibrium value S_0. A plot of $\log[S(t)-S_0]$ versus t was made and always found to be a straight line; T_{1p} was obtained from the slope. The rather long values (10 to 3000 sec) enabled us to measure T_{1p} in various H fields, but with a fixed frequency $\nu_n\approx85$ Mc/sec, by periodically switching back to the field $H_0=h\nu_n/g_n\beta$ for a sampling of the nmr signal. In this way the data in Figs. 11 and 12 were obtained for crystal No. 12, oriented with $\theta=90°$, $\varphi=0°$.

In these two figures the solid line is the equation

$$\frac{1}{T_{1p}}=\left[1.4\times10^{-16}H^3\coth\frac{g_\perp\beta H}{2kT}+\frac{1.25\times10^{12}}{H^2}\exp\left(\frac{-47}{T}\right)\right]\operatorname{sech}^2\left(\frac{g_\perp\beta H}{2kT}\right)+2.1\times10^{-4}T+\frac{7.5\times10^2T}{H^2}\ \text{sec}^{-1},\quad(30)$$

where $g_\perp=2.70$ and H is in Oe. We note that this single expression fits the data over a wide range of fields and temperatures. We interpret the terms as follows. The first two terms are proton relaxation by the Nd^{3+} ions: The field and temperature dependence is exactly that of Eq. (29) and even the constants are in surprisingly good agreement considering the many approximations made in the theory. The third term, necessary for a good fit at low temperatures and intermediate fields, is just that expected for relaxation from the direct process of a non-Kramers' doublet. Although $g=g_\perp=0$ for Pr^{3+} at $\theta=90°$, this term may still be attributed to a small Fe^{2+} impurity. The last term, necessary at the lowest fields and temperatures is more difficult to understand. The field dependence suggests cross relaxation with a paramagnetic impurity whose resonance begins to overlap that of the protons at low fields; but this should be temperature independent. Although we have, as yet, no reasonable explanation of this term, it is entirely negligible at the fields used in dynamic proton polarization.

Measurements of T_{1p} were also made on crystals Nos. 2 and 5, Table I, at $\theta=40°$, with the results of Figs. 13, 14, and 15. The angle φ was not determined in these experiments, but later measurements have shown that T_{1p} is essentially independent of φ. The

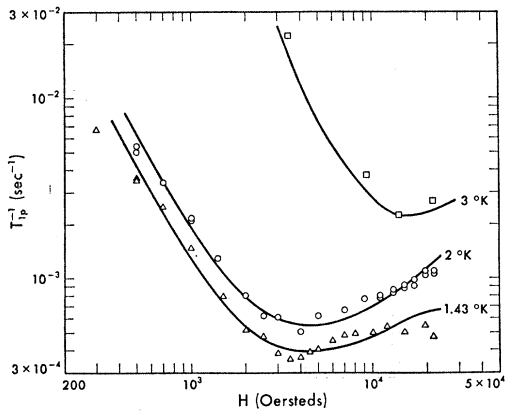

FIG. 12. Observed proton relaxation rate T_{1p}^{-1} versus H for the crystal of Fig. 11; the solid curves are given by Eq. (30).

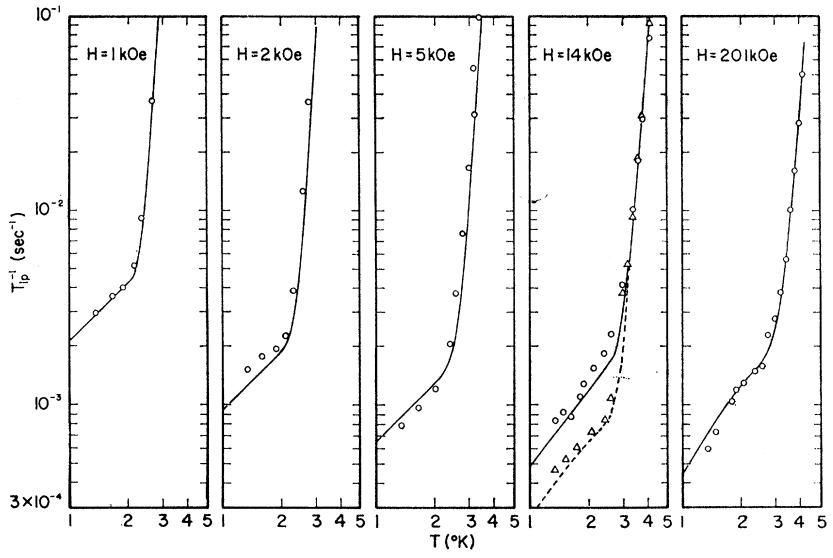

FIG. 13. Observed proton relaxation rate T_{1p}^{-1} versus T for 1% Nd in LaMN oriented with $\theta=40°$. ○—data for crystal No. 2, Table I; △—data for crystal No. 5, Table I. The solid curve is given by Eq. (31), the dashed curve by Eq. (32).

solid curve in Figs. 13 and 14, crystal No. 2, is the equation

$$\frac{1}{T_{1p}}=\left[2.16\times10^{-17}H^3\coth\left(\frac{g_{\mathrm{Nd}}\beta H}{2kT}\right)+\frac{1.5\times10^{12}}{H^2}\exp\left(\frac{-47}{T}\right)\right]\mathrm{sech}^2\left[\frac{g_{\mathrm{Nd}}\beta H}{2kT}\right]+\left[2.2\times10^{-8}H\coth\left(\frac{g_{\mathrm{Pr}}\beta H}{2kT}\right)\right]\mathrm{sech}^2\left(\frac{g_{\mathrm{Pr}}\beta H}{2kT}\right)+\frac{1.5\times10^{3}T}{H^2}\ \mathrm{sec}^{-1},\quad(31)$$

where H is in oersteds, $g_{\mathrm{Pr}}=g_{\parallel})_{\mathrm{Pr}}\cos\theta=1.19$ and $g_{\mathrm{Nd}}=[g_{\parallel}^2\cos^2\theta+g_{\perp}^2\sin^2\theta]^{1/2}=1.77$. Similarly, the curve in Fig. 15 and the dashed curve in Fig. 13, for crystal No. 5 is the equation

$$\frac{1}{T_{1p}}=\left[2.16\times10^{-17}H^3\coth\left(\frac{g_{\mathrm{Nd}}\beta H}{2kT}\right)+\frac{1.5\times10^{12}}{H^2}\exp\left(\frac{-47}{T}\right)\right]\mathrm{sech}^2\left(\frac{g_{\mathrm{Nd}}\beta H}{2kT}\right)+\left[1.1\times10^{-8}H\coth\left(\frac{g_{\mathrm{Pr}}\beta H}{2kT}\right)\right]\mathrm{sech}^2\left(\frac{g_{\mathrm{Pr}}\beta H}{2kT}\right)+\frac{1.1\times10^{3}T}{H^2}\ \mathrm{sec}^{-1}.\quad(32)$$

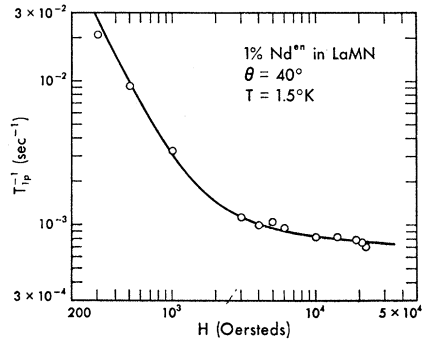

FIG. 14. Observed proton relaxation rate T_{1p}^{-1} versus H for crystal No. 2 (en=enriched). The curve is given by Eq. (31).

The first two terms in Eqs. (31) and (32) are the same and are interpreted as the relaxation due to the Nd^{3+} ions. To predict this we use Eq. (14), replacing $g_{\perp}$ by the actual value $g_{\mathrm{Nd}}=1.77$ and the measured value of T_{1e} at $\theta=40°$,[26] obtaining

$$\left(\frac{1}{T_{1p}}\right)_{\mathrm{Nd}}=\left[2.3\times10^{-17}H^3\coth\left(\frac{g_{\mathrm{Nd}}\beta H}{2kT}\right)+\frac{0.4\times10^{12}}{H^2}\exp\left(\frac{-47}{T}\right)\right]\mathrm{sech}^2\left(\frac{g_{\mathrm{Nd}}\beta H}{2kT}\right)\mathrm{sec}^{-1},\quad(33)$$

again in moderate agreement with the measurements.

Because of the field and temperature dependence of the third term in Eqs. (31), and (32) it is reasonable to ascribe it to a small impurity of Pr^{3+}, for which $g_{\parallel}=1.55$, $g_{\perp}=0$. From Eqs. (14) and (28), and assuming a Pr^{3+} concentration of 0.002%, we estimate for the direct

[26] G. Larson (to be published).

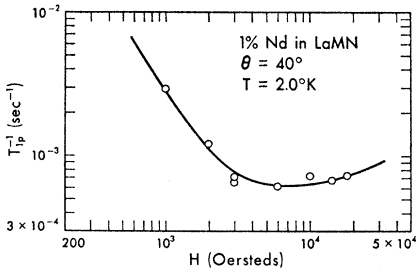

FIG. 15. Observed proton relaxation rate T_{1p}^{-1} versus H for crystal No. 5. The curve is given by Eq. (32).

process alone at $\theta=40°$

$$\left(\frac{1}{T_{1p}}\right)_{\mathrm{Pr}} \approx \left[2\times10^{-8}H\coth\left(\frac{g_{\mathrm{Pr}}\beta H}{2kT}\right)\right] \times\operatorname{sech}^2\left(\frac{g_{\mathrm{Pr}}\beta H}{2kT}\right)\mathrm{sec}^{-1}, \quad (34)$$

in good agreement with the third term of Eq. (31). The corresponding term for the crystal No. 5 can be explained with a 0.001% Pr impurity; these values are approximately those expected from the analyses of the chemicals used. The calculated proton relaxation from this amount of Pr due to the Raman and Orbach processes is entirely negligible. The last term in Eqs. (31) and (32), like that in (30), has yet no reasonable explanation.

The above interpretation of the data for crystals No. 2, 5, and 12 indicates that impurities other than Nd^{3+} have a significant contribution to the proton relaxation, and so an attempt was made to grow a purer crystal, No. 13, Table I, using higher purity chemicals. The measured relaxation data at $\theta=90°$ fit the form

$$\frac{1}{T_{1p}}=\left[2.5\times10^{-16}H^3\coth\frac{g_\perp\beta H}{2kT} +\frac{1.9\times10^{12}}{H^2}\exp\left(\frac{-47}{T}\right)\right]\operatorname{sech}^2\left(\frac{g_\perp\beta H}{2kT}\right) +4\times10^{-4}T+\frac{2.6\times10^2T}{H^2}\,\mathrm{sec}^{-1}. \quad (35)$$

The terms due to Nd are somewhat larger than Eq. (30), probably because the actual Nd concentration in the crystal was somewhat higher. The third and fourth terms, presumably due to impurities, are larger and smaller, respectively, than those of Eq. (30); we take this to indicate that crystal No. 13 was actually not significantly purer than the others.

Preliminary measurements[27] of T_{1p} for crystals Nos. 12 and 13 at temperatures down to $T=0.17°K$ at $\theta=90°$ and $H=8.3$ kOe yield data in moderate agreement with the expressions of Eqs. (30) and (35), respectively; the third term is dominant at the lowest temperatures. The relaxation rate for both crystals at 0.17°K was found to be $T_{1p}^{-1}\approx3\times10^{-5}$ sec^{-1} at 8.3 kOe.

[27] M. Schulz (private communication).

C. Diffusion Effects

The measurements in Sec. IV B are the first in which the proton and electron relaxation rates in crystals were both extensively measured over a wide range of fields and temperatures. Except for anomalies at low fields due to extraneous impurities the empirical relationship between T_{1p} and T_{1e} for Nd^{3+} is in surprisingly good agreement with the prediction of Eq. (14) for the simple shell-of-influence model. We have neglected up until now the important process of diffusion of nuclear polarization. What can happen is this: A proton near a Nd ion gets flipped by the relaxation process w_2 or w_3, or even by the microwave transition W_2 or W_3. It then may engage in a mutual spin flip with a proton a little farther away, which in turn flips the next proton, etc. There is a diffusion of proton polarization closely related to the random walk process: The mean-squared distance through which the polarization diffuses in time t is $\langle R^2\rangle\approx a^2W_{12}t/3$, where a is the spacing between protons, and W_{12} is the rate of mutual spin flip for two neighboring protons. This process was invoked[15] to explain how the distant nuclei in very magnetically dilute crystals could relax in a reasonable time.

Free diffusion is described by the equation

$$\partial p/\partial t=D\nabla^2p, \quad (36)$$

where $D=W_{12}a^2\approx10^{-13}$ cm^2 sec^{-1} for LaMN. Terms due to the relaxation through paramagnetic ions may be added to Eq. (36), with the final prediction for the proton relaxation rate[28,29]

$$\frac{1}{T_{1p}}=4\pi NbD\approx8.5N\left[\frac{3}{10}\left(\frac{g\beta}{H}\right)^2\frac{1}{T_{1e}}\right]^{1/4}D^{3/4}, \quad (37)$$

where $N=$number Nd^{3+} ions/cm^3, and it is assumed that the polarization freely diffuses for r greater than the scattering length $b=0.7\times[3(g\beta)^2/10H^2T_{1e}D]^{1/4}$, which has the typical value $b\sim1$ Å for Nd in LaMN at 10 kOe and 1.5°K. The magnitude of T_{1p}^{-1} predicted by Eq. (37) is $\sim10^3$ larger than what we observe; furthermore the dependence $T_{1p}^{-1}\propto H^{-1/2}T_{1e}^{-1/4}$ is certainly not observed. The reason that free-diffusion theory is not valid for our experiments is that at the relatively high concentration of 1% many of the protons are not on speaking terms, i.e., their local magnetic fields from the Nd ion are sufficiently different as to prevent rapid mutual proton spin flips. It is useful to define a diffusion barrier radius d at which the ion

[28] G. R. Khutsishvili, Akad. Nauk. Gruzin SSR, Inst. Fiz. 4, 3 (1956).
[29] P. G. de Gennes, J. Phys. Chem. Solids 7, 345 (1958).

field equals the dipole field of another proton

$$g_1\beta/d^3 \approx g_n\beta/a^3. \tag{38}$$

For $a=1.6$ Å (in the H_2O molecule) we find $d\approx 16$ Å. Thus $b \ll d$ in all our experiments, and Eq. (37) would not be expected to be valid.

We note that a prediction for retarded diffusion[30]

$$\frac{1}{T_{1p}} = \frac{3}{10}\left(\frac{g\beta}{H}\right)^2 \frac{1}{d^3 r_2^3}\frac{1}{T_{1e}} \tag{39}$$

yields rates too small by 10^2. Equation (39) is obtained from (14) with r_1 replaced by d on the assumption that all the protons at $r < d$ would be shifted out of the observed nmr resonance line; this is apparently not realistic in the present case.

Although the shell-of-influence model predicts reasonably well the observed average magnitude of the proton relaxation rate as well as the field and temperature dependence, it does not explain why the observed rate is unique rather than a distribution of rates depending on the proton distance from the ion. We note that although we have used $r_1=4.4$ Å and $r_2=24$ Å, appropriate for 1% Nd in LaMN, any other pair of radii r_1' and r_2', such that $r_1'r_2'=r_1r_2$, would of course equally well explain the data. As an alternate *ad hoc* model, suppose that protons within $r_1'=7$ Å are excluded from the observed resonance because their local field is greater than the nmr linewidth of 20 Oe. Further suppose that for protons outside $r_2'=d=16$ Å, rapid diffusion becomes possible to the numerous more distant protons, whose rate of relaxation is essentially limited by the same average value of $\bar{\sigma}$ in the zone $r_1'<r<r_2'$. This model would explain the observations. Undoubtedly the true situation is rather complex, with diffusion to the distant protons playing some role.

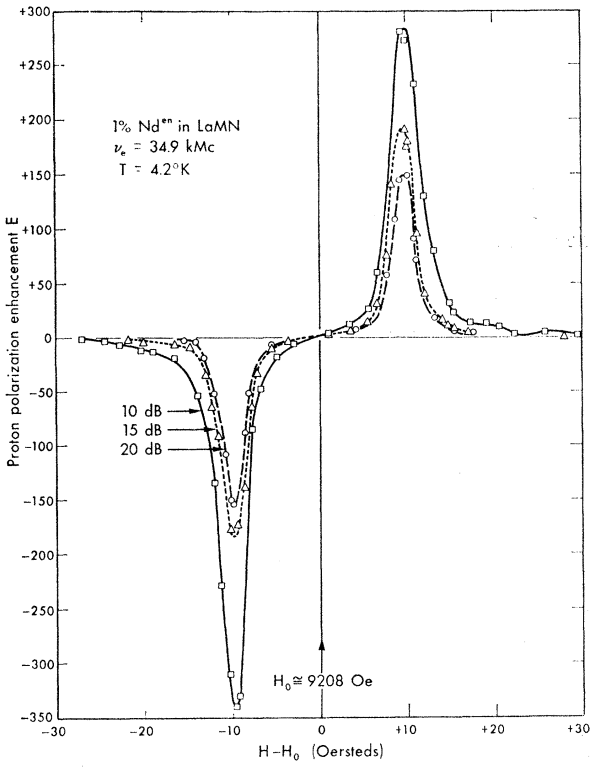

FIG. 16. Observed proton polarization enhancement [Eq. (42)] versus H for crystal No. 11, Table I, with $\theta=90°$, $\varphi=0$, at three settings of the microwave attenuator.

[30] W. E. Blumberg, Phys. Rev. **119**, 79 (1960).

V. DYNAMIC POLARIZATION OF PROTONS IN $(Nd,La)_2Mg_3(NO_3)_{12}\cdot 24H_2O$

1. *Procedures.* We have studied the dynamic proton polarization and its dependence on microwave power for the crystals of Table I at frequencies $\nu_e=35$, 50, and 74 kMc, in the temperature range $1.3<T<4.2$°K and in fields up to 20 kOe. Experiments were usually performed as follows. At a given temperature T and field in the vicinity of a forbidden resonance the proton thermal equilibrium signal was observed in the absence of microwave power by slowly sweeping ν_n. We recorded the peak-to-peak derivative signal S_0 as well as the integrated area A_0 under the absorption curve. The microwaves were then switched on with the waveguide switch, and the proton resonance continuously swept through as the polarization built up, reaching a steady state signal S_E, and measured area A_E. The procedure was repeated for different values of H. For small polarizations ($\bar{p}<0.3$) the enhancement, defined by

$$E_{\text{meas}}=S_E/S_0 \tag{40}$$

was used to calculate the measured proton polarization from

$$\bar{p}_{\text{meas}}=p_0E_{\text{meas}}=E_{\text{meas}}\times 2.4\times 10^{-5}\nu_n/T, \tag{41}$$

where ν_n is in Mc/sec, and T°K is the temperature at which S_0 was measured. Thus even though the microwaves raise the temperature, Eq. (41) still gives the correct proton polarization.

For larger polarizations the lineshape change requires that areas be compared to obtain the enhancement. If the nmr coil filling factor is large the proton resonance absorption itself will appreciably lower or raise the effective Q at enhanced positive or negative polarizations, which tends to make the recorded areas smaller or larger, respectively. This effect can be reduced by using a poor filling factor (at some sacrifice of signal-to-noise ratio) and corrections can be made by observing the fractional voltage change $\Delta V/V$ at the diode in Fig. 8. It can be shown that for $(\Delta V/V)<0.1$ a good approximation is

$$E_{\text{meas}}=(A_E/A_0)[1\pm(\Delta V/2V)], \tag{42}$$

which is the expression we have used to obtain the enhancements quoted.

2. *Enhancement measurements.* Figure 16 shows E_{meas}

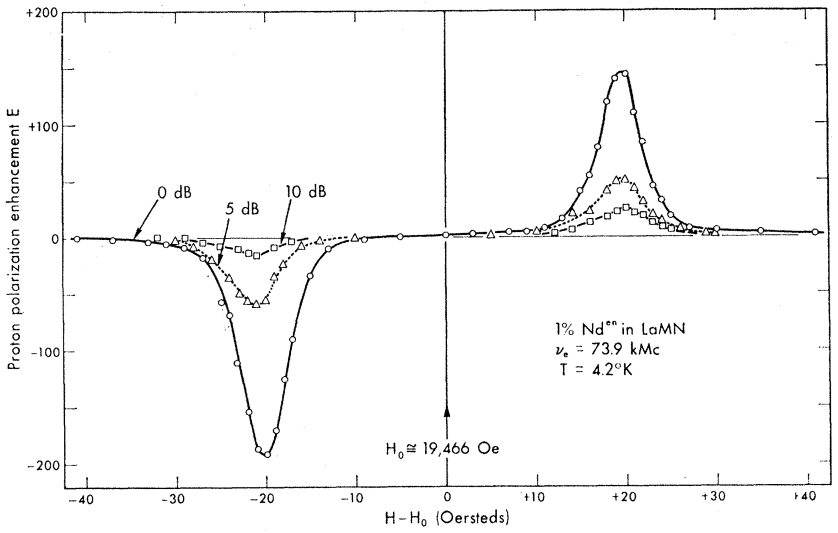

FIG. 17. Observed enhancement versus H for crystal No. 11, Table I, with $\theta=90°$, $\varphi=0$, at various microwave attenuator settings.

versus H for crystal No. 11, Table I, oriented with $\theta=90°$, $\varphi=0°$, at 34.9 kMc/sec and 4.2°K for three settings of the microwave power attenuator. The positive and negative enhancements are well resolved and separated, within experimental error, by the spacing $\Delta H=2Hg_n/g_1=20.7$ Oe as expected from Fig. 3(b). In measurement, as in the others, we did not always find the positive and negative enhancements to be equal. There is an apparent random variation of $\sim 10\%$ probably due to slow drifts in the apparatus, e.g., microwave frequency, power, cavity tuning, amplifier gain, etc. Also, Fig. 16 does not represent the optimum enhancement; at higher powers $E_{\text{meas}}=407$ was observed.

Similarly, Fig. 17 shows the enhancement for the same crystal measured at 73.9 kMc/sec and 4.2°K. The enhancement peaks are even better resolved and have the expected spacing. Although one expects larger enhancements than at 35 kMc/sec because of the better resolution, it is actually smaller in this particular run because the microwave power was insufficient.

Figure 18 shows E_{meas} versus H for crystal No. 6 at 74 kMc/sec and 1.5°K. This experiment showed for the first time that large enhancements ($E_{\text{meas}}\approx 510$) corresponding to large proton polarizations ($\bar{p}_{\text{meas}}\approx 0.68$) could actually be obtained. Later measurements in crystal No. 11 yielded $\bar{p}_{\text{meas}}=0.72$, to be compared to the theoretical ideal value $p_i=0.83$.

These results, as well as a number of others, are summarized in Table II. A not surprising general conclusion is that the polarization continues to increase the higher the frequency and the lower the temperature. There seems to be no marked difference between the results for natural and enriched Nd, although the statistics are not very good.

Some preliminary experiments were also done with other concentrations of Nd: at 5% and at 0.1% the enhancement was definitely smaller by a factor ~ 5; at 2.5% and 0.5% the enhancement was smaller by a factor ~ 2. Although our data are not extensive we conclude that a 1% concentration is approximately optimum.

3. *Power dependence of enhancement.* With H set on an enhancement peak, the enhancement was measured as a function of the microwave power delivered to the cavity, with the results shown in Fig. 19 for crystal No. 11 at 34.9 kMc/sec and in Fig. 20 for the same crystal at 73.9 kMc/sec. The solid curves are expressions of the form

$$E_{\text{meas}}=E_{\text{sat}}P/(P_{1/2}+P), \tag{43}$$

where E_{sat} is the enhancement obtainable at complete saturation, P is the cavity power (in mW) and $P_{1/2}$ is the power for half saturation. Equation (43) has the form of Eq. (17a) if we assume $P\propto s\propto H_{1e}^2$. Values of E_{sat} and $P_{1/2}$ were chosen in each case for a best fit to the data; the agreement is reasonable. At 34.9 kMc/sec the values of E_{sat} are found to be about half the ideal value, probably because of a slight overlap in the tails

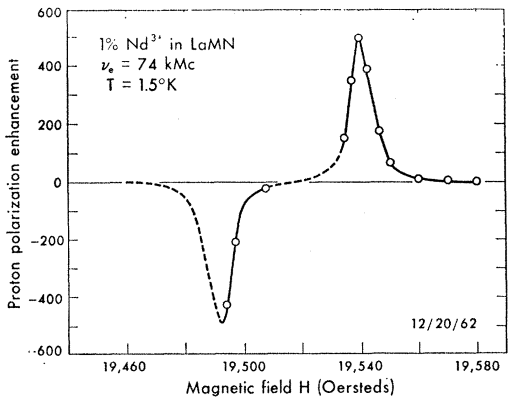

FIG. 18. Observed enhancement versus H for crystal No. 6, Table I, with $\theta=90°$, $\varphi=30°$. The positive enhancement corresponds to an actual proton polarization of 68%.

TABLE II. Results of dynamic proton polarization experiments in 1% Nd in LaMN, where θ is $\angle z'$, H; ν_e is the microwave frequency; H is the magnetic field; T is the temperature of helium bath at thermal equilibrium; E_{meas} from Eq. (40) or (42); p_0 is the thermal equilibrium proton polarization [Eq. (7d)]; p_{meas} from Eq. (41); p_i is the ideal proton dynamic polarization [Eq. (6)] at temperature T.

Crystal No. (Table I)	θ	ν_e kMc/sec	H kOe	T °K	E_{meas}	p_0 ($\times 10^{-4}$)	p_{meas}	p_i
1	30	35	17.7	2.1	+300	8.6	+0.26	+0.38
11	90	35	9.2	2.1	+460	4.5	+0.21	+0.38
11	90	35	9.2	4.2	+407	2.2	+0.09	+0.20
2	40	50	20	2.1	+400	9.7	+0.39	+0.51
2	40	50	20	1.35	−340	15.1	−0.51	−0.71
11	90	74	19.5	1.5	+540	13.3	+0.72	+0.83
11	90	74	19.5	4.2	+195	4.7	+0.09	+0.39
11	90	70	18.5	1.4	+490	13.5	+0.66	+0.83
11	90	70	18.5	1.4	−426	13.5	−0.57	−0.83
6	90	74	19.5	1.5	+510	13.3	+0.68	+0.83
6	90	74	19.5	1.5	−425	13.3	−0.57	−0.83

of the forbidden and allowed lines. At 73.9 kMc/sec and 1.5°K, $E_{\text{sat}}\approx 600$, compared to $E_{\text{ideal}}=620$. Thus we might have obtained $\bar{p}\approx 0.80$ with a more powerful klystron. Another shortcoming of our apparatus is insufficient helium pumping speed, limiting us to $T\approx 1.5$°K with 100 mW input. For the experiments in Table II, the average leakage factor $\bar{f}$ [Eq. (15b)] has been calculated using the measured values of T_{1e} and T_{1p} and $n/N=2400$, corresponding to 1% Nd. In all cases $\bar{f}<10^{-2}$, and so we conclude from Eq. (17a) that the extraneous proton relaxation has a negligible effect in limiting the maximum enhancement. In this sense Nd in LaMN is far superior to, say, irradiated plastics where $\bar{f}\sim 10$, typically, chiefly because of undesirable paramagnetic centers.[3]

In attempts to test the prediction in Sec. II B that a saturation factor $s_{1/2}\sim 10^3$ is required to reach half-maximum enhancement, we compared the power P_1 required to half saturate the main epr line with the power P_2 required to half saturate the enhancement at 35 kMc/sec and 1.5°K, with the cavity tuned to a very low Q mode. We found $P_2\sim 130P_1$, leading to $s_{1/2})_{\text{meas}}\sim 10^2$. This is admittedly a very rough measurement because of the phonon bottleneck and the uncertainty of the constancy of the cavity Q. However there is a definite indication that the microwave field partially breaks down the diffusion barrier, thus requiring less power than predicted by the elementary model.

4. *Polarization build-up.* In the same run in which the data for Fig. 19 were obtained, measurements were made of the proton polarization as it built up. We always found $\bar{p}(t)=\bar{p}_{\max}[1-\exp(-t/\tau_{\text{on}})]$, and a unique characteristic time τ_{on}. At both $T=2.1$°K and 4.2°K, for $P\lesssim P_{1/2}$, the data fit, with some scatter, the expression

$$\frac{1}{\tau_{\text{on}}}=\frac{1}{T_{1p}}\left[1+\frac{P}{P_{1/2}}\right], \qquad (44$$

where $P_{1/2}$ is the cavity power required for half-maximum enhancement. This form is expected from Eq. (19a), which simply predicts that $\tau_{\text{on}}=\frac{1}{2}T_{1p}$ at half-maximum enhancement. For $P>P_{1/2}$, τ_{on} did not seem to vary much with power. Similar measurements at 74 kMc/sec also fit a form like Eq. (44), with

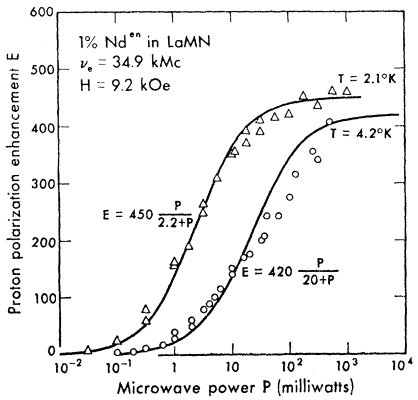

FIG. 19. Observed enhancement versus microwave power P delivered to the helium bath, for crystal No. 11, Table I, with $\theta=90°$, $\varphi=0$.

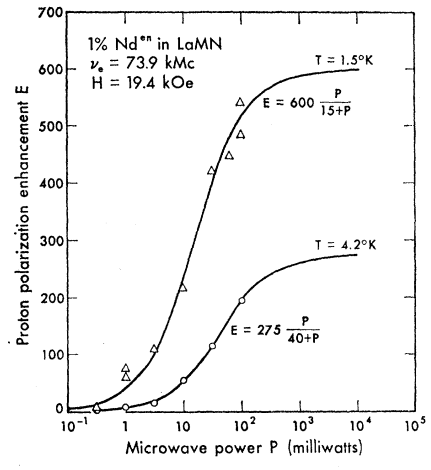

FIG. 20. Observed enhancement versus microwave power P delivered to the helium bath for crystal No. 11, Table I, with $\theta=90°$, $\varphi=0$.

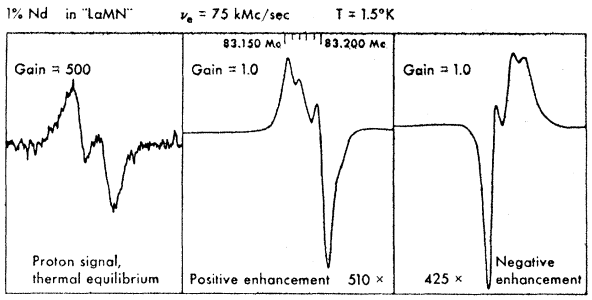

FIG. 21. Derivative of the proton nmr signal in crystal No. 6, with $\theta=90°$, $\varphi=30°$ at thermal equilibrium; positive enhancement, $E_{\text{meas}}\approx 510$; and negative enhancement, $E_{\text{meas}}=425$. The line structure is due to local proton-proton dipolar interaction.

$\tau_{\text{on}}\approx\frac{1}{2}T_{1P}$ at half maximum enhancement. However it was found that because of the scatter the data also could be fit to a form $\tau_{\text{on}}^{-1}=T_{1p}^{-1}(1+KP)^{1/4}$ expected from diffusion theory[1]; τ_{on} was found to depend critically on the exact resonance condition for the forbidden transition. Drifts of a few oersteds had an appreciable effect on τ_{on} and E_{meas}. It is worth noting that although the diffusion barrier d invalidates free diffusion theory for the proton relaxation in the absence of microwaves, when the microwaves are turned on, the Nd ions are flipped rapidly, and so d may become significantly smaller; this reduces the required saturation factor and weakens the dependence of τ_{on} on power.

5. *Line shapes.* For crystal No. 6, $\theta=90°$, $\varphi=30°$, Fig. 21 shows the derivative of the proton nmr signal at thermal equilibrium, at large positive enhancement, and at large negative enhancement. Figure 22 is for crystal No. 11, except with $\varphi=0°$; Fig. 23 shows the integrated signals of Fig. 22. We note the additional structure at high negative and positive polarizations. This is explained by Fig. 7b, which if inverted will display the predicted proton resonance spectrum at $\bar{p}=+1.0$ as the frequency ν_n is increased from left to right. The sharp lines on Fig. 23(b) are a replotting of Fig. 7(b) and explain qualitatively the structure seen.

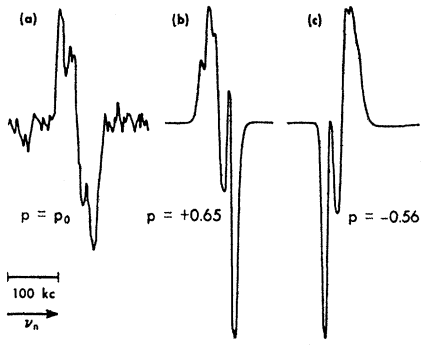

FIG. 22. Derivative of proton nmr signal in crystal No. 11, Table I, with $\theta=90°$, $\varphi=0$, at (a) thermal equilibrium, (b) positive enhancement, and (c) negative enhancement.

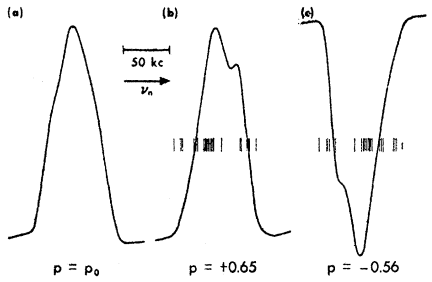

FIG. 23. Electronically integrated signals obtained from those of Fig. 22, and recorded simultaneously.

When $\bar{p}$ is made negative the structure is reflected through the center, as expected.

6. *Adiabatic reversal.* An experiment was performed in which the proton polarization was first enhanced parallel to the field direction, the microwaves then switched off, the field reduced to zero, and turned on in the opposite direction, all in a time $\sim$15 sec. It was then found that the proton polarization was parallel to the new field direction and had approximately half its original magnitude. This is an example of an adiabatic reversal,[31] which could be made quantitative in a faster cycle.

Another interesting feature, not yet fully understood, is the way the proton polarization dynamically reverses when the field is switched from one forbidden resonance to the other. The protons on one side of the nmr resonance line are reversed more rapidly than the others, probably because they are nearer a Nd^{3+} ion; the results indicate a transient microscopic distribution of both positive and negative polarizations.

7. *Summary and conclusions.* Because of the relatively sharp resonance lines, Nd^{3+} in LaMN is an excellent substance for dynamic polarization of the protons through dipolar coupling with the Nd ions. In high fields and frequencies (75 kMc/sec) polarizations approaching the ideal values may be obtained in the He^4 temperature range. At still higher frequencies, essentially complete polarization should be feasible, yielding a resolution of the local dipole-dipole structure in the proton resonance line. The proton relaxation, the enhancement, and its dependence on microwave power are reasonably consistently explained by a simple shell-of-influence model.

ACKNOWLEDGMENTS

We are greatly indebted to Dr. P. L. Scott for the preliminary measurements[32] which led us to undertake this study; to Kenneth Langley for much help in taking data; and to Dr. Norman Ford, J. R. McColl, and T. E. Gunter for calculations of dipole sums.

[31] R. V. Pound, Phys. Rev. **81**, 156 (1951); E. M. Purcell and R. V. Pound, *ibid.* **81**, 279 (1951).

[32] P. L. Scott, thesis, University of California, Berkeley, 1962 (unpublished).